The Structure of the Hydrated Electron. Part 1. Magnetic Resonance of Internally Trapping Water Anions: A Density Functional Theory Study

Ilya A. Shkrob

Chemistry Division, Argonne National Laboratory, 9700 South Cass Avenue, Argonne, Illinois 60439

Received: December 1, 2006; In Final Form: March 5, 2007

Density functional theory is used to rationalize magnetic parameters of hydrated electron trapped in alkaline glasses as observed using electron paramagnetic resonance (EPR) and electron spin echo envelope modulation (ESEEM) spectroscopies. To this end, model water cluster anions ($n = 4-8$ and $n = 20$, 24) that localize the electron internally are examined. It is shown that hyperfine coupling tensors of H/D nuclei in the water molecules are defined mainly by the cavity size and the coordination number of the electron; the water molecules in the second solvation shell play a relatively minor role. An idealized model of the hydrated electron (that is usually attributed to L. Kevan) in which six hydroxyl groups arranged in an octahedral pattern point toward the common center is shown to provide the closest match to the experimental parameters, such as isotropic and anisotropic hyperfine coupling constants for the protons (estimated from ESEEM), the second moment of the EPR spectra, and the radius of gyration. The salient feature is the significant transfer (10−20%) of spin density into the frontal O 2p orbitals of water molecules. Spin bond polarization involving these oxygen orbitals accounts for small, negative hyperfine coupling constants for protons in hydroxyl groups that form the electron-trapping cavity. In Part 2, these results are generalized for more realistic geometries of core anions obtained using a dynamic one-electron mixed quantum/classical molecular dynamics model.

1. Introduction

This paper continues a series of publications[1−4] on the "bottom up" approach to the structure of excess electron in polar solvents. In this two-part series, we consider the most important species of this kind: the hydrated electron, e_{hyd}^-.[5] We revisit the magnetic properties of the electron trapped in alkaline ice and compare ab initio and density functional theory (DFT) calculations of such properties for model internally trapping $(H_2O)_n^-$ ($n = 4-24$) clusters and hyperfine coupling (hfcc) tensors for magnetic nuclei that were determined experimentally in the 1970s and the 1980s (Section 2 and Appendix A). Although this comparison upholds several commonly assumed features for the cavity model of e_{hyd}^-, it also suggests that one-electron theories of the hydrated electron might be incomplete. The salient feature that is missing from these theories is the significant transfer (10−20%) of the spin density into the frontier O 2p orbitals of water molecules forming the solvation cavity. There have been recent suggestions[6,7] that this transfer might account for the observed 200 cm^{-1} downshift of the O−H stretch mode and ∼30 cm^{-1} downshift H−O−H bend modes in the resonance Raman spectra of e_{hyd}^- in liquid water (as well as a similar red shift in gas-phase water anion clusters).[8] The examination given in this paper and Part 2 of this study[9] suggest that the magnetic resonance properties of e_{hyd}^- cannot be understood in any other way.

Traditionally, solvated electrons were treated using one-electron models in which the excess electron is considered separately from the valence electrons in the solvent (which is described classically). In these models, the electron interacts with the solvent molecules by means of an ad hoc empirical, classical potential.[5] Since the 1980s, the hydrated electron has become the test bed for state-of-the-art path integral[10] and mixed quantum/classical molecular dynamics (MQC MD)[11−14] calculations in which the solvent motion is treated dynamically at the classical level, whereas a single particle, the excess electron, is treated quantum mechanically in the adiabatic[11,14] or nonadiabatic[11,12] approximations. The MQC MD approach allows one to treat the electron relaxation, diffusion, pump−probe dynamics, and excitation spectrum straightforwardly, with relatively few further assumptions. This approach proved to be both insightful and productive, and it greatly refined the theoretical picture of electron solvation. However, despite these many successes, the one-electron models, regardless of their technical sophistication, suffer from two closely related problems:

One of these problems is that of justification. It does not follow from any higher-level theory or a general principle that the one-electron models in which the solvent is described classically and a single electron is described quantum mechanically is the adequate picture of e_{hyd}^-. The reasoning goes the other way around. The one-electron model is *postulated* and then the consequences of this assumption are tested against the experiment. Good agreement with the experiment is then taken as the justification for the assumptions and simplifications introduced in the model. The pitfall of this approach is that more than one theory is capable of accounting for a given group of experimental observations, especially when empirical $e^-−H_2O$ pseudopotentials are allowed. The majority of theoretical studies of e_{hyd}^- have focused on a single property: the absorption spectrum in the visible. Despite great differences in the approach and the degree of detail, all of the 250+ theoretical papers on e_{hyd}^- claim good understanding of this spectrum and its salient features. A possible conclusion is that this absorption spectrum might not be too revealing about the details of electron solvation once the model satisfies a few rather general criteria. (In this regard, the ability of MCQ MD calculations[11−14] to address the basic features of pump−probe experiments on e_{hyd}^- is more

* To whom correspondence should be addressed. E-mail: shkrob@anl.gov.

10.1021/jp068278m CCC: $37.00
Published on Web 05/27/2007

important than the explanation of the static spectrum). What is more troubling is that similar one-electron models have been used[15] (with the same degree of fidelity) to account for the absorption spectra of the solvated electron in liquid ammonia and aliphatic amines, for which there is a strong case, supported by both theoretical considerations[1,16,17] and nuclear magnetic (NMR)[18,19] and electron paramagnetic resonance (EPR) spectroscopies (reviewed in ref 1), that the one-electron picture is incorrect, as most of the spin density is contained in the frontier N 2p orbitals of the solvent molecules in the first and the second solvation shells.[1,18] In other words, the one-electron models, even when these are demonstrably incorrect in their basic assumptions, still account quite well for the optical properties of the excess electron. Such observations bring to the fore the question of how justifiable such one-electron models are in general.[1−4]

One way to justify and support these models would be calculating the less frequently addressed properties of e_{hyd}^-. Therein lies the second pitfall of the one-electron models, since by their very nature these are not conducive to such tests. In particular, the two experimental methods that give the most direct and detailed structural information on the ground state of the solvated/trapped electron—magnetic resonance data for trapped electrons in alkaline ices (Section 2) and resonance Raman spectroscopy of hydrated electrons in liquid water[6]—are the least tractable from the standpoint of these theories, because the solvent molecules can no longer be considered classically. Other properties of e_{hyd}^- that do not lend themselves easily to such calculations are its vacuum UV band at 190 nm[20] and the proton-transfer reactions.[5] The 190 nm band supposedly involves O 2p orbitals in the water molecules forming the cavity,[20] whereas the latter requires full quantum mechanical treatment of water molecules. A limited set of experimental results is revisited repeatedly, whereas other equally important properties of e_{hyd}^- remain seldom addressed.

Over the past decade, this situation has changed, largely due to the advances in anion cluster chemistry. The need for understanding the properties of gas phase $(H_2O)_n^-$ anions[21] has fomented interest in modeling such species using ab initio and DFT methods that go beyond the one-electron approximation.[22−24] Such calculations were originally carried out for relatively small clusters ($n = 6-10$) that trap the electron at their surface, yielding dipole-bound anions. The internally trapped electrons can also be modeled using such small clusters,[24] but their structure does not correspond to any known species observed experimentally in the gas phase. Recently, the increased computational power allowed to examine several larger clusters ($n = 20$ and 24) that demonstrate internal solvation by four dangling HO groups[22,23] (while most of the remaining OH groups are involved in the H-bond formation). Other promising developments were the recent Car−Parrinello[25] and hybrid[26] multielectron MD modeling of the e_{hyd}^- in liquid water based on the use of pseudopotentials for valence electrons in water molecules.

Most of these studies focused on the energetics of the water anion clusters. Yet the approach also allows one to estimate the magnetic parameters for the ^{1}H and ^{17}O nuclei in the water molecules and compare these estimates with EPR parameters for trapped electron in alkaline ice. Such is the program implemented in this paper. The results of EPR, electron spin echo envelope modulation (ESEEM), ^{1}H electron nuclear double resonance (ENDOR) and electron-electron double resonance (ELDOR) spectroscopy of trapped electrons in alkaline ice are critically reviewed in Appendix A in the Supporting Information, and the main conclusions are summarized in Section 2. For the benefit of the reader, the basics of EPR and ESEEM spectroscopies pertaining to the observations of the trapped electron are discussed in Appendix B in the Supporting Information.

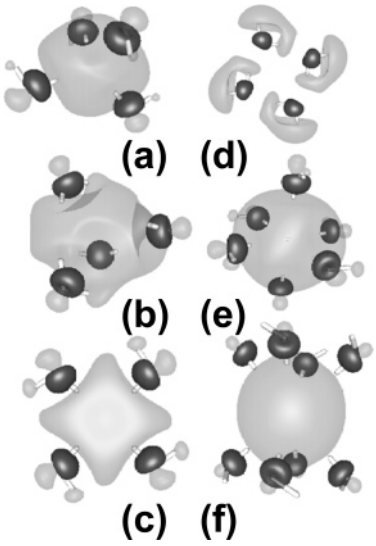

Figure 1. Isodensity maps for singly occupied molecular orbit (SOMO) of (a) b-type and (b) d-type D_{2d} symmetrical tetrahedral water anions and planar C_{4h} symmetrical (c) b-type and (d) H-bonded square water anions, (e) C_i symmetrical octahedral and (f) D_4 symmetrical cube-shaped b-type water anions ($\pm 0.03\ a_0^{-3}$ surfaces are shown; light shade is for positive, dark shade is for negative). In (e), the negative part is shared between the O 2p orbitals of six or eight water molecules forming the cavity. B3LYP/6-311++G** model for $X-H_a$ distance of 2.1 Å (optimized geometry).

The magnetic resonance studies of water ices[27−47] culminated in the well-known octahedral model of e_{hyd}^- (Figure 1e) that is associated with the name of L. Kevan,[27] although it was first suggested by Natori and Watanabe[28] and Natori.[29] In this model, the cavity is formed by six non-hydrogen-bonded (NHB) hydroxyl groups pointing toward the common center. In fact, neither Kevan's EPR, ENDOR, and ESEEM studies[27,30−34] nor the follow-up ESEEM studies pursued by Bowman's and Tsvetkov's groups[35−37] lend *direct* support to this model. Surprisingly, the first solid evidence that this model does capture, albeit approximately, the *magnetic* properties of the e_{hyd}^- is provided by this study. To reduce the length of the paper, the Sections, Tables, and Figures with the designator "S" (e.g., Figure 1S) are placed in the Supporting Information.

2. Magnetic Resonance Studies

We refer the reader to Appendices A and B in the Supporting Information for the detailed review of magnetic resonance of trapped electrons and the basics of the techniques involved, respectively. Very briefly, the goal of the EPR[45] and ESEEM[37] studies is to provide hyperfine coupling (hfcc) tensors for magnetic ^{1}H (or ^{2}H) nuclei in the OH groups lining the solvation cavity. These tensors can be used to map the singly occupied molecular orbital (SOMO) and determine (within certain approximations) the geometry of the solvation cavity. The hyperfine coupling tensor **A** with principal values of (A_{xx}, A_{yy}, A_{zz}) can be represented as $(a + B_{xx}, a + B_{yy}, a + B_{zz})$, where a is the isotropic hyperfine coupling constant (originating through the Fermi contact interaction) and **B** is the traceless tensor of anisotropic hyperfine interaction that originates through electron−nuclear magnetic dipole coupling. Typically, such tensors are nearly axial, so that $B_{xx} \approx B_{yy} \approx T_\perp$ and $B_{zz} \approx -2T_\perp$. For a point like an electron interacting with a nucleus at a distance r, $T_\perp = \gamma_e\gamma_n/hr^3$, where γ_e and γ_n are the corresponding gyro-

magnetic ratios, and h is the Plank constant. For a proton, $B_{zz}^{H} \approx 57.6/r^3$,[37] where the distance is given in Å and the hfcc's are in Gauss (1 G = 10^{-4} T). All of the EPR and ESEEM data for trapped electrons were interpreted using this point dipole approximation, although it is not obvious that the latter holds for a cavity occupied by a spatially extended electron wavefunction.[46] The r_{XH} distances (where H denotes the nearest proton and X is the centroid of the electron density in the cavity) were estimated from the experimentally determined $T_\perp$ using this approximation. Only in retrospect was it realized[46] that this approximation might result in incorrect values for r_{XH} when the latter is in the range of 2.1−2.4 Å (i.e., in the range suggested by the ESEEM data).[37] The situation is further complicated when there is nonzero spin density on O atoms, because the protons would also interact with the unpaired electron in the O 2p orbitals. This interaction decreases both the dipolar contribution and the isotropic constant, and it can reverse the sign of a^H, via "spin bond polarization,"[48] which is spin polarization of the protons through the framework of σ bonds involving unpaired electron density in p orbitals of the heteroatom.[1,16,17,45]

Because EPR spectra of the trapped electron in alkaline ices are structureless,[42−44] these spectra provide the estimate of the "total" magnetic coupling that is given by the second moment M_2 of the resonance line; the proton contribution to the latter is ∼23 G^2 in the alkaline ices (eq B5 in Appendix B). Assuming that the protons are magnetically equivalent and the coordination number n is known, these estimates can be refined using "flip-flop satellites;"[33] for $n = 5$, this analysis gives $|a| = 2 \pm 3$ G and $2T_\perp = 8.3 \pm 1$ G (which corresponds to $r_{XH} \approx 1.98$ Å). Neither EPR nor ESEEM provide the direct estimate of the mean coordination number, n; rather, these spectroscopies provide the constraints on the dipole coupling of the electron. Originally, ESEEM data were interpreted as supportive of Kevan's model with six equivalent protons and $a^H \approx +2.1$ G (for $r_{XH} \approx 2.1$ Å).[27] The positive isotropic hfcc for the protons was consistent with one-electron models. However, subsequent ESEEM studies[36,37] indicated that, in fact, $a^H \approx -0.92$ G (for $r_{XH} \approx 2.01$ Å). The negatively valued constants originate through spin bond polarization involving unpaired electrons in the O 2p orbitals. Negatively valued isotropic hfcc constants were also observed using NMR and dynamic nuclear polarization for protons in ammoniated electron.[1,18,19] These results signify *the breakdown of the one-electron approach*. The same is also suggested by the anomalously small absolute value of the hfcc constant. In the absence of spin bond polarization, large positively valued estimates for a^H (∼3−5 G) were suggested by semicontinuum models.[28,49] Since the initial experiments seemed to yield such large, positive hfcc constants, these experiments were considered to be supportive of such one-electron models. The subsequent ESEEM experiments,[36,37] however, yielded hfcc estimates that are clearly incompatible with these one-electron models. By contrast, the early tight-binding ab initio calculations for water anions[16,17,50] yielded *negative* proton constants.

The original estimate of six (equivalent) protons[27] was later revised to two protons at 2 Å and 7−8 protons at 3.5 Å,[36,37] although the latter estimate appears to be incompatible with the constraints imposed by the observed EPR line width. Yet another constraint is imposed by the second moment of the EPR line in ^{17}O substituted ices, which is ∼134 G^2 for 37% at ^{17}O.[34] Schlick et al.[34] estimated from this parameter that the total transfer of the spin density into the O 2p orbitals is ∼10−16%.

Far from being able to provide direct structural information, the magnetic resonance data themselves need to be understood and interpreted.

3. Computational Details

In this study, gas-phase water cluster anions were analyzed mainly using density functional theory models with the B3LYP functional (Becke's exchange functional[51] and the correlation functional of Lee, Yang, and Parr)[52] from Gaussian 98.[53] B-LYP functionals are most frequently used to estimate isotropic hfcc in radicals and radical ions, for which it typically yields accurate and reliable results.[54,55] As a complementary approach, self-consistent field Hartree−Fock (HF) and second-order Møller-Plesset (MP2) perturbation theory[56] calculations were used. The latter two methods gave very similar estimates for *magnetic* parameters, so in most cases, only HF results are discussed below. Although the anisotropic hfcc's calculated using these DFT and ab initio methods were comparable, the isotropic hfcc's differed substantially: the HF and MP2 generally yield smaller absolute isotropic hfcc's (a^O) for ^{17}O nuclei and larger isotropic hfcc (a^H) for the innermost ^{1}H nuclei, as compared to DFT methods (such as B-LYP and LSDA). This difference can be traced to the fact that the DFT models better account for the spin polarization effects[55] (which accounts for their preferred use for the calculations of EPR parameters).[54,55]

Unless specified otherwise, the basis set was a 6-31G split-valence, double-ζ Gaussian basis set augmented with diffuse and polarized (d, p) functions (6-311++G**). Very similar results were obtained using two other basis sets, augmented Dunning's correlation consistent double basis set (aug-cc-pVDZ)[57] and Barone's triple-ζ basis set[58] with diffuse functions and an improved s-part that was introduced specifically for the hfcc calculations (EPR-III). Reduction of the basis set to 6-31+G** or smaller sets gave rather different results from those obtained using these basis sets (see, for example, Tables 1S and 4S). That was not the case in ammonia clusters examined in our previous study.[1] This is because in water anion clusters, the spin density inside the cavity is substantially greater than in the ammonia clusters, and more diffuse sets are required to obtained reliable estimates. This is an important point, because the early ab initio studies[16,17] of water tetramer anions related to EPR used tight 3-21G and 4-31G basis sets. We also used basis sets (6-31+G** sets complemented by diffuse functions for hydrogen and oxygen atoms) that were developed by Bradforth and Jungwirth[59] and Herbert and Head-Gordon[23] for ab initio modeling of water anion clusters. The hfcc tensors obtained using these basis sets were very similar to those obtained using the standard 6-311++G** set.

In most of these calculations, a ghost atom (i.e., a floating-center set of diffuse functions) was added with parameters used in refs 23 and 59. For the 6-311++G** set and other large basis sets, the introduction of this ghost atom had little effect on the calculated hfcc tensors.

Three types of the model clusters were examined: (i) small, highly symmetrical $(H_2O)_n^-$ clusters ($n = 4$, 6, and 8) in which water molecules were arranged in such a way that the hydroxyl group of each molecule pointed toward the common center, X (b-type clusters), or with the water dipoles pointing to the same center (d-type clusters); (ii) four $n = 20$ and 24 clusters that internally trap electrons (the cluster geometries were obtained from Khan[22] and Herbert and Head-Gordon;[23] the geometries of these clusters are given in Appendix D in the Supporting Information); and (iii) embedded clusters generated from 1000 snapshots of the e_{hyd}^- obtained in a 100 ps long MQC MD trajectory (Part 2).

In addition to the hfcc tensors, second moments M_2^H and M_2^O were calculated for ^{1}H and ^{17}O nuclei, respectively, using eq B7 (the contributions from isotropic and anisotropic parts of

the hfcc tensor were calculated separately). We also used these hfcc parameters and the directional cosines for hfcc tensors to directly simulate EPR spectra for randomly oriented fixed-geometry clusters (assuming a spherical *g*-tensor). For small, highly symmetrical clusters, the simulated EPR spectra exhibited some structure, but the spectra simulated for $n = 20$ and $n = 24$ anion clusters (for both $^1H_2{}^{16}O$ and $^1H_2{}^{17}O$) are nearly Gaussian and show no spectrally resolved resonance lines, such as the experimental spectra obtained in alkaline glasses. Typical examples of such spectra are shown in Figure B1a in the Supporting Information.

SOMO density maps indicate that the electron wavefunction inside the cavity and in the frontier orbitals of O atoms have opposite signs (Figure 1), suggesting a way to distinguish these two contributions. Typically, the diffuse, positive part of SOMO occupies 80−90% of the geometrical cavity at a density of $+(0.03-0.05)a_0^{-3}$ and less than 10% at a density of $+(0.07-0.1)a_0^{-3}$ (where $a_0 \approx 0.53$ Å is the atomic unit of length). In large clusters, ∼50−60% of the total SOMO density is contained inside the sphere centered at *X* corresponding to the closest of the NHB hydrogens (that is subsequently denoted as H_a); at least 75% of the total density is contained within the 3 Å sphere. The highest (negative) density is found in the frontal O 2p orbitals of oxygen atoms in the first solvation shell. These general observations do not depend on which computational method (DFT, HF, or MP2) is used to calculate the SOMO.

Throughout the next section, no attention is paid to the energetics of the electron solvation, as clearly the effects of interaction of such model clusters with the solvent in liquid water would greatly exceed any correction from advanced treatment of correlation or polarization effects. We are mainly interested in the structural aspects and the salient features of the ground state SOMO. *Our goal is to find which minimal multielectron model produces the features that are compatible with diverse experimental observations for the* e_{hyd}^-.

The radius of gyration, r_g, for the electron given below is defined as $r_g = \langle r^2 - \langle r \rangle^2 \rangle$. We used SOMO for this averaging. In the one-electron model, the gyration radius can be roughly estimated from the optical spectrum moment analysis for the s → p absorption band, as described by Bartels;[60] the typical estimate is 2.5 Å. The total spin density, ϕ_{2p}^O, in the O 2p orbitals of water was defined (consistently with the typical way in which such a parameter would be experimentally determined in EPR spectroscopy) as the sum of $|B_{zz}^O/B_{zz}^O(\text{at.})|$ taken over all oxygen-17 nuclei. For the same cluster geometry, the estimates for this parameter obtained using different methods were comparable (see Figures 2a and 4a in Section 4.1).

4. Results and Discussion

4.1. Small, Symmetrical Anions ($n = 4$, 6, and 8). Small water anion clusters observed experimentally in the gas phase either do not attach the electron or yield surface-bound electrons.[21] The resulting species are of great theoretical interest but provide limited insight into the structure of the trapped electron in liquids and glasses. Previous ab initio and DFT studies[16,17,22−24] suggest that internal solvation is possible when several (at least four) NHB hydrogens form a "solvation cavity." By contrast, H-bonded protons play almost no role in the electron solvation. The simplest anion cluster that has the desired properties is a tetrahedral (D_{2d} symmetrical) b-type cluster shown in Figure 1a (the Natori model of "solvated electron").[16,17,28] This cluster (for the optimized geometry) has the lowest energy in the B3LYP/6-31+G** model; however, for larger basis sets (6-311++G** and aug-cc-VDZ), a C_{4h} symmetrical planar ring (Figure 1d) has the lowest energy (the relative energies for these two clusters and the D_{2d} symmetrical d-type cluster (Figure 1b) and C_{4h} b-type planar cluster (Figure 1c) are given in Table 1S). The energy switchover upon extension of the basis set follows the change from external to internal solvation. Despite considerable variation of the structure, all of these b- and d-type tetramer anions exhibit $a^O \approx -(18-24)$ G and a^H that is negative and small (for NHB hydroxyl groups). For D_{2d} symmetrical b-type clusters (Figure 1a), the comparison of hfcc parameters obtained using various methods is given in Table 2S. All of these methods yield a ground state that exhibits a diffuse positive density at the center (observe that the wavefunction is aspherical) complemented by negative density in the frontal lobes of the O 2p orbitals (Figure 1a). Depending on the method and the basis set, the r_{XH} distance (between the wavefunction centroid at X and the closest proton, H_a) varies between 1.45 Å (LSDA/aug-cc-pVDZ) and 3.2 Å (HF/aug-cc-pVDZ); for a given basis set, this distance is always longer for the HF method than for the B3LYP and MP2 methods (which yield similar optimized geometries). Since the size of the cluster largely defines the overlap of the SOMO wavefunction with the nuclei, comparing the hfcc parameters obtained for different optimized structures is not instructive. To facilitate such a comparison, we have calculated several parameters for D_{2d} symmetrical clusters as a function of the $X-H_a$ distance, r_{XH}, optimizing all other degrees of freedom. The results are shown in Figures 2−6.

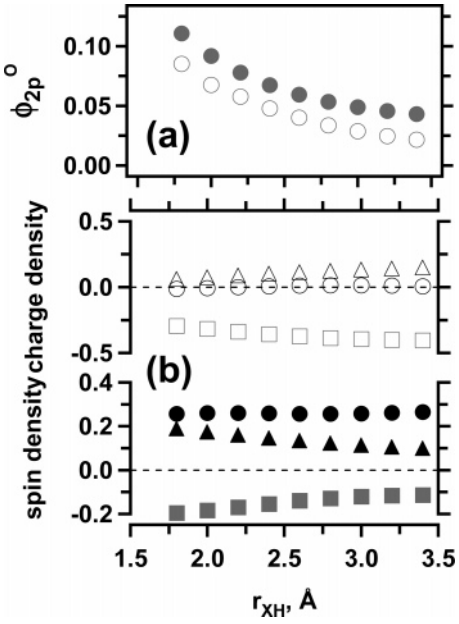

Figure 2. (a) Total population ϕ_{2p}^O of oxygen 2p orbitals (filled circles, to the left) as a function of r_{XH}, the $X-H_a$ distance (B3LYP/6-311++G** calculation for the D_{2d} symmetrical b-type water anion shown in Figure 1a). For comparison, the same parameters calculated using HF/6-311++G** method are shown in the same panel (open circles). (b) Mulliken population analysis: atomic charge (filled symbols, top) and spin (open symbols, bottom) densities for H_a (circles), H_b (triangles), and O (squares).

As the cavity size increases from 1.8 to 3.2 Å, the total spin density, ϕ_{2p}^O, in the O 2p orbitals decreases from 0.11 to 0.04 (Figure 2a), and the Mulliken spin density on oxygen atoms decreases from −0.2 to −0.1 (B3LYP/6-311++G** model; Figure 2b). The atomic spin density on the H_a protons is negative, which immediately suggests that $a^H < 0$. The isotropic hfcc's a^O on oxygen-17 and the protons decrease exponentially with r_{XH}, from −25 to −14 G and −0.8 to −0.2 G, respectively

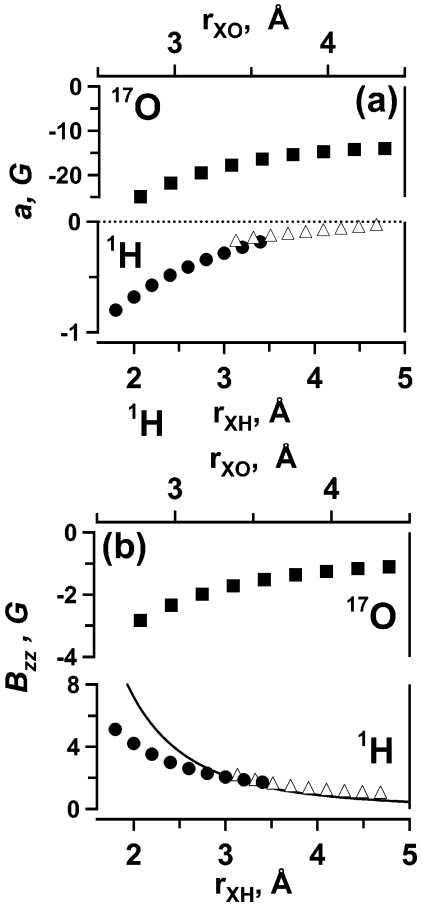

Figure 3. (a) Isotropic hfcc's for ^{17}O (filled squares; to the top) and ^{1}H (bottom) nuclei (the H_a [filled circles] and H_b [open triangles] nuclei are shown together) vs $X-$O and $X-H_{a,b}$ distances, respectively. Solid lines are exponential fits (B3LYP/6-311++G** calculation for b-type tetrahedral water anion). (b) The same as (a) for the *zz* principal component of anisotropic hfcc tensor. The solid line is the estimate obtained in the point-dipole approximation, eq (B9).

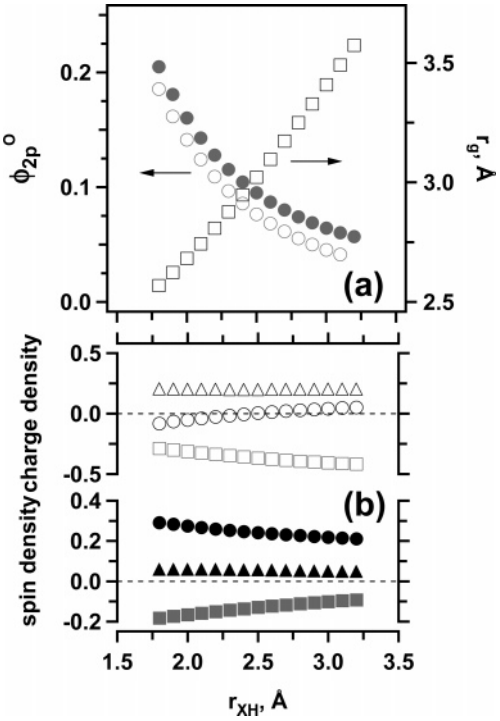

Figure 4. (a) Total population ϕ_{2p}^{O} of oxygen 2p orbitals (filled circles, to the left) and radius of gyration, r_g (open squares, to the right), as a function of r_{XH} and the $X-H_a$ distance (B3LYP/6-311++G** model for the octahedral water anion shown in Figure 1e). For comparison, ϕ_{2p}^{O} calculated using the HF/6-311++G** method are shown in the same panel (open circles). (b) Mulliken population analysis: atomic charge (filled symbols, top) and spin (open symbols, bottom) densities for H_a (circles), H_b (triangles), and O (squares) atoms.

(Figure 3a). Observe that a^H is small and negative for all cavity sizes. The isotropic and anisotropic hfcc's for H_a and H_b protons plotted vs the distance r_{XH} to these nuclei follow the same general dependence (Figure 3). Only for $r_{XH} > 3$ Å does the constant B_{zz}^H approach the estimate given by the point-dipole approximation (solid line in Figure 3b); at shorter distances the anisotropic hfcc is significantly lower than this point-dipole estimate. The estimates for B_{zz}^H (as is the case for all other water anions) obtained using B3LYP and HF methods are very close (Figure 1S in the Supporting Information). For $r_{XH} \approx 2$ Å, $B_{zz}^H \approx 4$ G instead of 7.2 G in the point dipole approximation (panels b in Figures 3 and 1S). To obtain the experimental estimate of ≈7 G, the $X-H_a$ distance should be <1.5 Å, which is unrealistic. The experimental a^H (−0.93 G)[36,37] can be matched only for $r_{XH} < 1.6$ Å (Figure 3a). Thus, the tetrahedral arrangement seems to be excluded by our results. This is also suggested by Figure 2S that shows the plot of the contribution to the second moment from the protons, M_2^H. For $r_{XH} \approx 1.8-2$ Å, this parameter is only 10−15 G^2, which is significantly smaller than the experimental 21−23 G^2.[32,22,36] This is due to the smallness of the anisotropic contribution (Figure 3a); the isotropic contribution to the EPR line width is negligible.

In the HF model with the same basis set, the isotropic hfcc on the protons is several times more negative than in the B3LYP model (for H_a changing from −5.2 G to −1.4 G when the $X-H_a$ distance changes from 1.8 to 3.2 Å). Such estimates are clearly incompatible with the experimental ones. For isotropic hfcc constants on oxygen-17, the HF methods always yield a^O's that are 20−100% less negative than B3LYP, resulting in smaller estimates for M_2^O (which is dominated by these isotropic hfcc's). Either way, the latter parameter is a few thousands of G^2, which is significantly greater than 360 G^2 given by Schlick et al.[34] (see Section 2). All of these considerations suggest that tetrahedral sites for e_{hyd}^- are rejected by EPR and ESEEM results. The same reasoning excludes d-type tetrahedral clusters of the type shown in Figure 1b (Figure 3S in the Supporting Information summarizes various calculated parameters). Our conclusion is in full accord with MQC MD[10−14] and other[26] simulations indicating that the coordination number of the electron is close to 6. We have examined such clusters for two reasons. First, all large anion clusters known to trap the electron internally from previous ab initio and DFT studies have tetrahedral core anions. As shown below, having more water molecules around this core anion cluster does not qualitatively change the analysis given above. Second, it is clearly seen that the number of nearby water molecules has to be relatively large, so the analysis of Astashkin et al.[36] suggesting just two water molecules in the first solvation shell cannot be correct.

We turn to the octahedral complexes shown in Figure 1e (Kevan's model). Such complexes are expected to resemble most closely the "real" hydrated electron in liquid water. There are important differences between the results for octa- and tetrahedral complexes. These differences are traceable to the greater sphericity of the electron wavefunction and more extensive spin sharing in the larger anions (as seen from Figure 4a). First, the B_{zz}^H more closely follow the point-dipole model (Figure 5b); thus, it is possible to match the experimental estimate of this

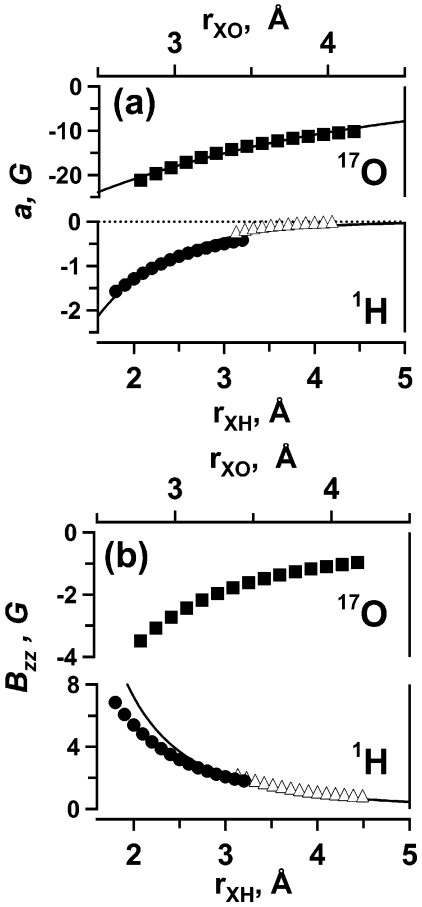

Figure 5. (a) Isotropic hfcc's for ^{17}O (filled squares; to the top) and ^{1}H (bottom) nuclei (the H_a [filled circles] and H_b [open triangles] nuclei are shown together) vs $X-O$ and $X-H_{a,b}$ distances, respectively. Solid lines are exponential fits (B3LYP/6-311++G** calculation for the octahedral water anion). (b) The same as (a) for *zz* principal component of anisotropic hfcc tensor, B_{zz}^{H}. The solid line is the estimate obtained in point-dipole approximation (eq B9).

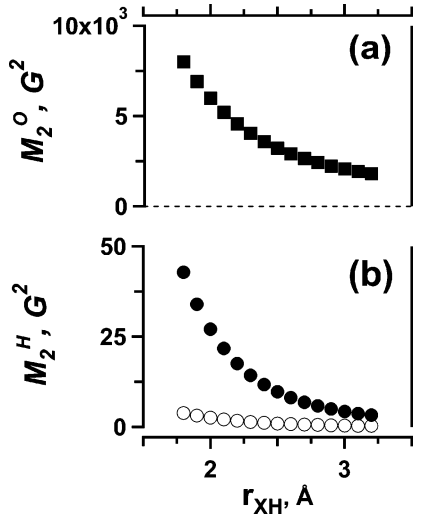

Figure 6. Second moments of EPR spectra for the octahedral water anion (B3LYP/6-311++G** model) vs the cavity size (the $X-H_a$ distance). (a) The contribution from the ^{17}O nuclei (filled squares, top) and (b) the proton contribution (filled circles, bottom); in the latter, the (small) contribution from isotropic hfcc is shown by empty circles.

parameter for an $X-H_a$ distance of 1.8−2 Å. Matching of the experimental a^{H} [36] is possible for $r_{XH} \approx 2-2.1$ Å (Figure 5a), and matching of the experimental M_2^H gives $r_{XH} \approx 2$ Å (Figure 6). As shown in Appendix C and Figure 4S, downshifts of H−O−H bending and O−H stretching modes in such clusters approach the experimentally observed magnitude for the same r_{XH}. Thus, all three EPR parameters for the protons and the vibrational downshifts can be simultaneously matched for the same cavity geometry. This matching is possible only in the DFT models: as was the case with the tetrahedral clusters, HF and MP2 methods grossly overestimate a^H, yielding for realistic cavity sizes ($r_{XH} < 2.5$ Å) negative hfcc's of several Gauss, values that are excluded by ESEEM spectroscopy.[36,37] Furthermore, large a^H would increase M_2^H to 50−80 G^2, which is inconsistent with EPR results. The estimate for M_2^O is ∼5000 G^2 (Figure 6, ∼3000 G^2 in the HF model), which suggests a line width, ΔB_{pp}, of ∼140 G (for fully oxygen-17-substituted e_{hyd}^-). The energy minimum is at $r_{XH} \approx 2.1$ Å in the B3LYP model (see the SOMO maps in Figure 1e) and ∼3 Å in the HF model.

Figure 4a shows the cavity size dependence for the total population ϕ_{2p}^{O} of O 2p orbitals and the gyration radius, r_g. As r_{XH} increases from 1.8 to 3.2 Å, the spin density transferred to oxygen atoms decreases from 0.20 to 0.05, and the gyration radius r_g increases from 2.4 to 3.6 Å (B3LYP/6-311++G** model). Once more, the experimental $r_g \approx 2.5$ Å[60] is matched for $r_{XH} \approx 1.9-2.0$ Å (Figure 4a). Figure 4b shows the cavity size dependence for atomic spin and charge densities obtained by Mulliken population analysis. As the cavity increases, the charge on H_a and O in the hydroxyl groups gradually approaches its value for individual water molecules (in the same model), +0.25 and −0.5 *e*. At $r_{XH} \approx 2$ Å, the corresponding atomic charges are −0.05 and −0.31 *e*, and the atomic spin densities are +0.27 and −0.17, respectively (the spin density is always negative for H_a protons).

Finally, we briefly consider the results obtained for two cube-shaped $n = 8$ water anions: a D_4 symmetrical b-type anion shown in Figure 1f and the corresponding C_{4h} symmetrical d-type anion (see Figure 5S for the summary of EPR parameters). Since the former anion has a high degree of sphericity, the point approximation does not break down, even for $X-H_a$ distances as short as 2 Å. The degree of spin transfer to O 2p orbitals is greater than in the octahedral and tetrahedral anions ($\phi_{2p}^{O} \approx 0.3$ for $r_{XH} \approx 1.8$ Å). The isotropic constants a^H are not too different from those for octahedral anions; since the coordination number is greater, the second moment is too large: $M_2^H \approx 48$ G^2 (vs experimental 21−23 G^2)[32,33,36] for $r_{XH} \approx 2$ Å. Even for the d-type anion (in which the electron is solvated by both OH groups of the water molecule), the isotropic hfcc's on the protons are small and negative (∼−1 G for $r_{XH} \approx$ 2−2.5 G). When ^{17}O constants estimated for these anions are plotted against r_{XO}, the hfcc's for both types of clusters follow each other, suggesting that a^O is mainly a function of the $X-O$ distance rather than molecule orientation. From the standpoint of EPR parameters, the major difference between the b- and d-orientation appears to be in the anisotropic constants for the inner protons: while for the b-type anion, the point approximation is accurate, for the d-type anion (and this refers to all anion clusters that we examined), B_{zz}^H is significantly smaller than the estimate obtained in the point dipole approximation (Figure 5S). Consequently, the estimates for this parameter become unrealistically small, and d-orientation of water molecules is not supported by our simulations.

All of these results provide strong support for Kevan's octahedral model[27−29] with the preferential orientation of H−O groups toward the center of the solvation cavity. This model, despite its being a gross idealization of e_{hyd}^- , appears to capture

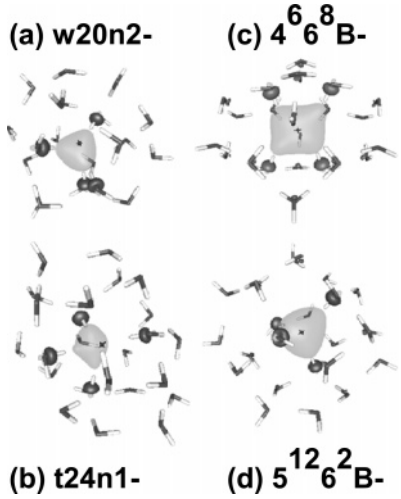

Figure 7. As Figure 1, for the internally trapping large water anions (EPR parameters, for optimized geometry given in Appendix D, are given in Tables 3S and 4S). The density levels are $\pm 0.03\ a_0^{-3}$ (light is for positive, dark is for negative): (a) w20n2, (b) t24n1 (c) $4^6 6^8$B and (d) $5^{12} 6^2$B anions. The cross indicates the position of a "ghost" atom inside the cavity.

several important features that are observed for the hydrated electron. However, using this model for *quantitative* simulation of ESEEM spectra (rather than the extracted "mean" hfcc's) gives poor results. The structure of e_{hyd}^- is neither regular nor octahedral; there is considerable variation in the coordination number, orientation of water molecules, etc. Many such conformations should be averaged to obtain the distributions of observable parameters. That is done in Part 2 of this study.[9]

4.2. Large Anions ($n = 20$ and $n = 24$). An $n = 20$ cluster (w20n2 anion found by Khan)[22] and three $n = 24$ clusters (t24n1 cluster found by Khan[22] and $4^6 6^8$B and $5^{12} 6^2$B anions found by Herbert and Head-Gordon)[23] were examined using B3LYP and HF methods (Figure 7). The electron in these clusters is bound internally by four NHB hydroxyl groups: for the $4^6 6^8$B anion, these OH groups are arranged in a rectangle; for the other three clusters, the arrangement is tetrahedral. The mean distance $\langle r_{XH} \rangle$ to the nearest hydroxyl protons is 1.78, 1.87, 2.21, and 2.16 Å, respectively (Table 3S). Remarkably, for these large cluster anions, even relatively tight binding basis sets (such as 6-31+G**) give estimates for *average* ^{17}O and ^{1}H hfcc constants that are comparable to the averages obtained using more diffuse basis sets (Table 4S). Isotropic hfcc's for protons are small ($|a^H| < 1$ G): either slightly negative or slightly positive (Table 3S). That relates only to DFT calculations (Table 3S); with the HF method, as was the case for smaller water anions, one obtains a large negative a^H of $-(5-8)$ G (Table 4S). Consequently, the estimates for M_2^H are >100 G^2 for Khan's[22] clusters (5 times greater than the experimental estimates). On the other hand, the estimates for M_2^H obtained using B3LYP method for $4^6 6^8$B and $5^{12} 6^2$B anions are <10 G^2, which is unrealistically small. This is due to the large cavity size (as compared to Khan's clusters) and small coordination number. Only for w20n2 and t24n1 anions (for which $\langle r_{XH} \rangle <$ 1.85 Å) is B_{zz}^H for the nearest protons close to the experimental value; for larger clusters ($r_{XH} >$ 2.16 Å), $B_{zz}^H < 4$ G. For other than the nearest four protons, the isotropic hfcc's are very small ($|a^H| < 0.05$ G for B3LYP method; $a^H < 0.2$ G for the HF method; see Tables 3S and 4S), that is, the excess electron is localized in the first solvation shell. The isotropic hfcc's for oxygen-17 nuclei suggest the same: for ^{17}O nuclei in the first solvation shell, the mean a^O ranges from -24.5 to -17.2 G (decreasing in absolute value for larger cavities), whereas for the second solvation shell, these constants range from -3 to -4 G. The total population of O 2p orbitals, despite this partial spin transfer to the second shell oxygen atoms, is quite small (as was the case for tetrahedral cavities examined in Section 4.1), $\sim 0.1-0.14$. Atomic spin densities for these oxygens are also small ($(1-5) \times 10^{-3}$ vs -0.05 for NHB hydroxyl groups.). Thus, the degree of electron density penetration beyond the first solvation shell is too small to have a significant effect on the second moment M_2^O from oxygen-17, that is similar to those for isolated tetrahedral clusters with the same r_{XH} (compare Table 3S and Figure 2S).

The comparison of EPR parameters for these large cluster anions with smaller tetrahedral anions obtained by retaining only the four water molecules forming the "solvation cavity" suggests that the effect of the second solvation shell on these EPR parameters is quite small. The second solvation shell is important for maintaining the fortuitous orientation of water molecules and obtaining the correct energetics; the EPR parameters, by contrast, depend mainly on the interaction of the excess electron density with *the nuclei in the first solvation shell.* This relatively tight localization of the SOMO justifies the use of the embedded cluster approach suggested in Part 2 of this series.[9]

5. Conclusion

This study aims to explain EPR/ESEEM parameters observed for trapped electrons in low-temperature alkaline ices. General considerations and experimental data (Section 2 and Appendix A) suggest that such an explanation cannot be sought using familiar one-electron models of electron solvation. Hence, ab initio and DFT methods were used to calculate hyperfine coupling tensors for water anion clusters that internally localize the electron via interaction with 4−8 NHB hydroxyl groups. Both small ($n = 4-8$) and large ($n = 20$, 24) model cluster anions were examined. For small clusters, the effects of coordination number and cavity size were studied. The comparison of small tetrahedral clusters with larger clusters identified by Khan[22] and Herbert and Head-Gordon,[23] in which the electron is 4-coordinated, suggests that the electron wave function is localized mainly over this first solvation shell, and thus, these small clusters are representative of the ones in the bulk water (this line of reasoning is continued and extended in Part 2). Examination of these small clusters suggests that 10−20% of the spin density is transferred into the frontal O 2p orbitals of the hydroxyl groups forming the cavity. This transfer has several consequences for the hfcc parameters. First, as a result of spin bond polarization, it makes isotropic hfcc's on the protons small and negative, in agreement with the ESEEM data of Astashkin et al.[36] Second, for clusters with low coordination number, it introduces significant lowering of anisotropic hfcc's, as compared to point-dipole approximation, as was anticipated by Golden and Tuttle.[46] Because the cavity sizes were determined using the latter approximation,[27,33,36,37] our results indicate the limited import of such estimates. Third, there is a very significant spin density on oxygen, suggesting that EPR results of Schlick et al.[34] for ^{17}O substituted glasses (used to justify the one-electron models) were compromised, as was also suggested by subsequent studies by the same authors.[61]

Although the one-electron point-dipole octahedral (Kevan's) model[27−29] might be overly simplistic, it turns out that such b-oriented octahedral arrangement of water molecules does capture several experimentally observed features of e_{hyd}^-; ironically, that occurs *only* in the multielectron model of the core anion. The isotropic and anisotropic hfcc tensor parameters

determined from ESEEM spectra,[36,37] the second moments of the EPR spectra,[32,33,36] the downshifts of the H−O−H bend and H−O stretch modes (see Appendix C),[6,7] the gyration radius of the electron,[60]—all these parameters can be quantitatively accounted for in such an octahedral model for $r_{XH} \approx 2-2.2$ Å. The DFT model thus provides rationalization for all of the experimental observables involving the *ground state* wave function of e_{hyd}^-.

Since MQC MD calculations[11−14] indicate that the coordination number of the hydrated electron is ∼6, our results suggest that the octahedral model is correct "on average." Although e_{hyd}^- does not have a regular solvation shell, like the idealized cluster anions examined in Section 4, this average does not look too dissimilar to the octahedral model, if one looks at mean parameters. This is demonstrated in Part 2 of this study.[9] Although the magnetic parameters for different trapping sites show considerable variation, the mean values are similar to the ones obtained in simple cluster models provided that the mean cavity size is the same. This is, again, due to the highly localized nature of the ground state electron wavefunction.

In many ways, the picture of the excess electron in water that emerges from the DFT model is similar to the familiar one-electron picture of this species: a large fraction of the excess electron density (∼50−60% of the SOMO) is contained inside the cavity, NHB hydroxyl groups stabilize the electron, there is little spin density in the hydroxyl protons, and the electron wavefunction in the cavity has s-character. Yet it also departs from this picture. A substantial fraction (10−20%) of the spin density is in the oxygen atoms of these NHB groups, so e_{hyd}^- can be viewed as a multimer radical anion.[1,2,18] That fraction is smaller for e_{hyd}^- than for the ammoniated electron,[1] in which most of the spin density is in the N 2p orbitals: the hydrated electron is, perhaps, the closest one can get to the one-electron picture; hence, the remarkable success of the latter in rationalizing the experimental observations.

Acknowledgment. I thank B. J. Schwartz, S. E. Bradforth, R. Larsen, D. M. Bartels, J. M. Herbert, A. Khan, and W. Domcke for many useful discussions and M. C. Sauer, Jr. for careful reading of the manuscript. This work was supported by the Office of Science, Division of Chemical Sciences, US-DOE under contract number DE-AC-02-06CH11357.

Supporting Information Available: A single PDF file containing Appendices A−D, Tables 1S to 4S, and Figures 1S−5S with captions. This material is available free of charge via the Internet at http://pubs.acs.org.

References and Notes

(1) Shkrob, I. A. *J. Phys. Chem. A* **2006**, *110*, 3967.
(2) Shkrob, I. A.; Sauer, M. C., Jr. *J. Phys. Chem. A* **2006**, *110*, 8126.
(3) Shkrob, I. A.; Sauer, M. C., Jr. *J. Phys. Chem. A* **2005**, *109*, 5754; *J. Chem. Phys.* **2005**, *122*, 134503.
(4) Shkrob, I. A.; Sauer, M. C., Jr. *J. Phys. Chem. A* **2002**, *106*, 9120. See also Shkrob, I. A.; Takeda, K.; Williams, F. *J. Phys. Chem. A* **2002**, *106*, 9132. Xia, C.; Peon, J.; Kohler, B. *J. Chem. Phys.* **2002**, *117*, 8855.
(5) Hart, E. J.; Anbar, M. *The Hydrated Electron*; Wiley-Interscience: New York, 1970.
(6) Tauber, M. J.; Mathies, R. A. *Chem. Phys. Lett.* **2002**, *354*, 518; *J. Phys. Chem. A* **2001**, *105*, 10952; *J. Am. Chem. Soc.* **2003**, *125*, 1394.
(7) Mizuno, M.; Tahara, T. *J. Phys. Chem. A* **2001**, *105*, 8823; **2003**, *107*, 2411. Mizuno, M.; Yamaguchi, S.; Tahara, T. In *Femtochemistry and Femtobiology*; Martin, M. M., Hynes, J. T., Eds.; Elsevier: Amsterdam, The Netherlands, 2004.
(8) Herbert, J. M.; Head-Gordon, M. *J. Am. Chem. Soc.* **2006**, *128*, 13293.
(9) Shkrob, I. A.; Glower, W.; Larsen, R.; Schwartz, B. J. *J. Phys. Chem. A* **2006**, In press.
(10) Schnitker, J.; Rossky, P. J. *J. Chem. Phys.* **1986**, *86*, 3471. Wallqvist, A.; Thirumalai, D.; Berne, B. J. *J. Chem. Phys.* **1986**, *86*, 6404. Romero, C.; Jonah, C. D. *J. Chem. Phys.* **1988**, *90*, 1877. Wallqvist, A.; Martyna, G.; Berne, B. J. *J. Phys. Chem.* **1988**, *92*, 1721. Miura, S.; Hirata, F. *J. Phys. Chem.* **1994**, *98*, 9649.
(11) Schnitker, J.; Rossky, P. J.; Kenney-Wallace, G. A. *J. Chem. Phys.* **1986**, *85*, 2989. Rossky, P. J.; Schnitker, J. *J. Phys. Chem.* **1988**, *92*, 4277. Schnitker, J.; Motakabbir, K.; Rossky, P. J.; Friesner, R. A. *Phys. Rev. Lett.* **1988**, *60*, 456. Webster, F. J.; Schnitker, J.; Frierichs, M. S.; Friesner, R. A.; Rossky, P. J. *Phys. Rev. Lett.* **1991**, *66*, 3172. Webster, F. J.; Rossky, P. J.; Friesner, R. A. *Comp. Phys. Comm.* **1991**, *63*, 494. Motakabbir, K.; Schnitker, J.; Rossky, P. J. *J. Chem. Phys.* **1992**, *97*, 2055. Murphrey, T. H.; Rossky, P. J. *J. Chem. Phys.* **1993**, *99*, 515.
(12) Schwartz, B. J.; Rossky, P. J. *J. Chem. Phys.* **1994**, *101*, 6917; *J. Phys. Chem.* **1994**, *98*, 4489; *Phys. Rev. Lett.* **1994**, *72*, 3282; *J. Chem. Phys.* **1994**, *101*, 6902. Rosenthal, S. J.; Schwartz, B. J.; Rossky, P. J. *Chem. Phys. Lett.* **1994**, *229*, 443.
(13) Wong, K. F.; Rossky, P. J. *J. Phys. Chem. A* **2001**, *105*, 2546.
(14) Borgis, D.; Staib, A. *Chem. Phys. Lett.* **1994**, *230*, 405. Staib, A.; Borgis, D. *J. Chem. Phys.* **1995**, *103*, 2642. Borgis, D.; Staib, A. *J. Chem. Phys.* **1996**, *39*, 1628; *J. Chem. Phys.* **1996**, *104*, 4776; *J. Phys.: Condens. Matter*. **1996**, *8*, 9389. Staib, A.; Borgis, D. *J. Chem. Phys.* **1996**, *104*, 9027. Borgis, D.; Bratos, S. *J. Mol. Struct.* **1997**, *1997*, 537. Nicolas, C.; Boutin, A.; Levy, B.; Borgis, D. *J. Chem. Phys.* **2003**, *118*, 9689.
(15) Ogg, R. A. *J. Am. Chem. Soc.* **1940**, *68*, 155; *J. Chem. Phys.* **1946**, 14, 114 and 295; *Phys. Rev.* **1946**, *69*, 243 and 668. Jortner, J. *J. Chem. Phys.* **1959**, *30*, 839. Kestner, N. R. In *Electrons in Fluids*; Jortner, J., Kestner, N. R., Eds.; Springer-Verlag: New York, 1973; pp 1. Sprik, M.; Impey, R. W.; Klein, M. L. *J. Chem. Phys.* **1985**, *83*, 5802. Sprik, M.; Impey, R. W.; Klein, M. L. *Phys. Rev. Lett.* **1986**, *56*, 2326. Sprik, M.; Klein, M. L. *J. Chem. Phys.* **1989**, *91*, 5665; *J. Chem. Phys.* **1988**, *89*, 1592. Marchi, M.; Sprik, M.; Klein, M. L. *J. Phys. Chem.* **1990**, *94*, 431. Rodriguez, J.; Skaf, M. S.; Laria, D. *J. Chem. Phys.* **2003**, *119*, 6044.
(16) Newton, M. D. *J. Phys. Chem.* **1975**, *79*, 2795.
(17) Clark, T.; Illing, G. *J. Am. Chem. Soc.* **1987**, *109*, 1013.
(18) Symons, M. C. R. *Chem. Soc. Rev.* **1976**, *5*, 337.
(19) Thompson, J. C. *Electrons in Liquid Ammonia*; Clarendon Press: Oxford, 1976.
(20) Nielsen, S. O.; Michael, B. D.; Hart, E. J. *J. Phys. Chem.* **1976**, *80*, 2482.
(21) Ayotte, P.; Johnson, M. A. *J. Chem. Phys.* **1997**, *106*, 811; *J. Chem. Phys.* **1999**, *110*, 6268. Weber, J. M.; Kim, J.; Woronowicz, E. A.; Weddle, G. H.; Becker, I.; Cheshnovsky, O.; Jophnson, M. A. *Chem. Phys. Lett.* **2001**, *339*, 337. Coe, J. V.; Lee, G. H.; Eaton, J. G.; Arnold, S.; Sarkas, H. W.; Bowen, K. H.; Ludewigt, C.; Haberland, H.; Worsnop, D. *J. Chem. Phys.* **1990**, *92*, 3980. Coe, J. V.; Earhart, A. D.; Cohen, M. H.; Hoffman, G. J.; Sarkas, H. W.; Bowen, K. H. *J. Chem. Phys.* **1997**, *107*, 6023. Verlet, J. R. R.; Bragg, A. E.; Kammrath, A.; Chesnovsky, O.; Neumark, D. M. *Science* **2005**, *307*, 93; *Science* **2004**, *306*, 669. Paik, D. H.; Lee, I-R.; Yang, D.-S.; Baskin, J. C.; Zewail, A. H. *Science* **2004**, *306*, 672. Headrick; Diken, E. G.; Roscioli, J. R.; Weddle, G. H.; Johnson, M. A. *Science* **2004**, *306*, 675. Hammer, N. I.; Roscioli, J. R.; Johnson, M. A. *J. Phys. Chem. A* **2005**, *109*, 7896 and references therein.
(22) Khan, A. *Chem. Phys. Lett.* **2005**, *401*, 85; *J. Chem. Phys.* **2003**, *118*, 1684; *J. Chem. Phys.* **2003**, *121*, 280.
(23) Herbert, J. M.; Head-Gordon, M. *J. Phys. Chem. A* **2005**, *109*, 5217; *Phys. Chem. Chem. Phys.* **2006**, *8*, 68.
(24) Kim, K. S.; Park, I.; Lee, K.; Cho, K.; Lee, J. Y.; Kim, J.; Joannopoulos, J. D. *Phys. Rev. Lett.* **1996**, 76, 956. Kim, K. S.; Lee, S.; Kim, J.; Lee, J. Y. *J. Am. Chem. Soc.* **1997**, *119*, 9329. Lee H. M.; Kim, K. S. *J. Chem. Phys.* **2002**, *117*, 706. Lee, H. M.; Suh, S. B.; Kim, K. S. *J. Chem. Phys.* **2003**, *118*, 9981; *J. Chem. Phys.* **2003**, *119*, 187. Lee, H. M.; Suh, S. B.; Tarakeshwar, P.; Kim, K. S. *J. Chem. Phys.* **2005**, *122*, 044309.
(25) Boero, M.; Parrinello, M.; Terakura, K.; Ikeshoji, T.; Liew, C. C. *Phys. Rev. Lett.* **2003**, *90*, 226403.
(26) Park, I.; Cho, K.; Lee, S.; Kim, K. S.; Joannopoulos, J. D. *Comp. Mater. Sci.* **2001**, *21*, 291.
(27) Narayana, P. A.; Bowman, M. K.; Kevan, L.; Yudanov, V. F.; Tsvetkov, Yu. D. *J. Chem. Phys.* **1975**, *63*, 3365.
(28) Natori, M.; Watanabe, T. *J. Phys. Soc. Jpn.* **1966**, *21*, 1573.
(29) Natori, M. *J. Phys. Soc. Jpn.* **1968**, *24*, 913; **1969**, *27*, 1309.
(30) Helbert, J.; Kevan, L.; Bales, B. L. *J. Chem. Phys.* **1972**, *57*, 723.
(31) Yoshida H.; Feng. D.-F.; Kevan, L. *J. Chem. Phys.* **1973**, *58*, 3411.
(32) Bales, B. L.; Helbert, J.; Kevan, L. *J. Phys. Chem.* **1974**, *78*, 221.
(33) Bales, B. L.; Bowman, M. K.; Kevan, L.; Schwartz, R. N. *J. Chem. Phys.* **1975**, *63*, 3008.
(34) Schlick, S.; Narayana, P. A.; Kevan, L. *J. Chem. Phys.* **1976**, *64*, 3153.
(35) Dikanov, S. A.; Tsvetkov, Yu. D.; Astashkin, A. V.; Bowman, M. K. *Chem. Phys. Lett.* **1983**, *94*, 231.
(36) Astashkin, A. V.; Dikanov, S. A.; Tsvetkov, Yu. D. *Chem. Phys. Lett.* **1988**, *144*, 258.

(37) Dikanov S. A.; Tsvetkov, Yu. D. *Electron Spin Echo Envelope Modulation (ESEEM) Spectroscopy*; CRC Press: Boca Raton, 1992; Chapter 133, pp 244−251.

(38) Bednarek, J.; Plonka, A.; Hallbrucker, A.; Mayer, E.; Symons, M. C. R. *J. Am. Chem. Soc.* **1996**, *118*, 9378; *Radiat. Phys. Chem.* **1998**, *53*, 635; *J. Phys. Chem. A* **1998**, *102*, 9091; *Phys. Chem. Chem. Phys.* **2000**, *2*, 1587.

(39) (a) Gillis, H. A.; Quickenden, T. I. *Can. J. Chem.* **2001**, *79*, 80 and references therein. (b) Johnson, J. E.; Moulton, G. C. *J. Chem. Phys.* **1978**, *69*, 3108. (c) Hase, H.; Kawabata, K. *J. Chem. Phys.* **1976**, *65*, 64.

(40) de Haas, M. P.; Kunst, M.; Warman, J.; Verberne, J. B. *J. Phys. Chem.* **1983**, *87*, 4089 and 4096.

(41) Nilsson, G. *J. Chem. Phys.* **1972**, *56*, 3437.

(42) Bennett, J. E.; Mile, B.; Thomas, A. *J. Chem. Soc*. **1967A**, 1393; **1969**, 1502.

(43) Ershov, B. G.; Pikaev, A. K. *Radiat. Eff.* **1969**, *2*, 135.

(44) Ohno, K.; Takemura, I.; Sohma, J. *Chem. Phys.* **1972**, *56*, 1202.

(45) Atkins, P. W.; Symons, M. C. R. *The Structure of Inorganic Radicals*; Elsevier: Amsterdam, 1967.

(46) Golden, S.; Tuttle, T. R., Jr. *J. Phys. Chem.* **1984**, *88*, 3781.

(47) Kroh, J.; Noda, S.; Yoshida, K.; Yoshida, H. *Bull. Chem. Soc. Jpn.* **1978**, *51*, 1961. Zagorski, Z. P.; Grodkowski, J.; Bobrowski, K. *Radiat. Phys. Chem.* **1980**, *15*, 343; *Chem. Phys. Lett.* **1978**, *59*, 533. Kondo, Y.; Aikawa, M.; Sumioshi, T.; Katayama, M.; Kroh, J. *J. Phys. Chem.* **1980**, *84*, 2544. Wolszczk, M.; Wypych, M.; Tomczyk, M.; Kroh, J. *Res. Chem. Intermed.* **2002**, *28*, 537.

(48) Chipman, D. *Theor. Chem. Acc.* **1990**, *82*, 93.

(49) Fueki, K.; Feng. D.-F.; Kevan, L. *J. Phys. Chem.* **1970**, *74*, 1977. Fueki, K.; Feng. D.-F.; Kevan, L.; Christoffersen, R. E. *J. Phys. Chem.* **1971**, *75*, 2297. Fueki, K.; Feng. D.-F.; Kevan, L. *J. Am. Chem. Soc.* **1973**, *95*, 1398. Feng. D.-F.; Ebbing, D.; Kevan, L. *J. Chem. Phys.* **1974**, *61*, 249.

(50) Noell, J. O.; Morokuma, K. *Chem. Phys. Lett.* **1975**, *36*, 465.

(51) Becke, A. D. *Phys. Rev. A: At., Mol., Opt. Phys.* **1988**, *38*, 3098.

(52) Lee, C.; Yang, W.; Parr, R. G. *Phys. Rev. B: Condens. Matter Mater. Phys.* **1988**, *37*, 785.

(53) Frisch, M. J.; Trucks, G. W.; Schlegel, H. B.; Scuseria, G. E.; Robb, M. A.; Cheeseman, J. R.; Zakrzewski, V. G.; Montgomery, J. A., Jr.; Stratmann, R. E.; Burant, J. C.; Dapprich, S.; Millam, J. M.; Daniels, A. D.; Kudin, K. N.; Strain, M. C.; Farkas, O.; Tomasi, J.; Barone, V.; Cossi, M.; Cammi, R.; Mennucci, B.; Pomelli, C.; Adamo, C.; Clifford, S.; Ochterski, J.; Petersson, G. A.; Ayala, P. Y.; Cui, Q.; Morokuma, K.; Malick, D. K.; Rabuck, A. D.; Raghavachari, K.; Foresman, J. B.; Cioslowski, J.; Ortiz, J. V.; Stefanov, B. B.; Liu, G.; Liashenko, A.; Piskorz, P.; Komaromi, I.; Gomperts, R.; Martin, R. L.; Fox, D. J.; Keith, T.; Al-Laham, M. A.; Peng, C. Y.; Nanayakkara, A.; Gonzalez, C.; Challacombe, M.; Gill, P. M. W.; Johnson, B. G.; Chen, W.; Wong, M. W.; Andres, J. L.; Head-Gordon, M.; Replogle, E. S.; Pople, J. A. *Gaussian 98*, revision A.1; Gaussian, Inc.: Pittsburgh, Pennsylvania, 1998.

(54) Lund, A.; Lindgren, M.; Lunell, S.; Maruani, J. In *Molecules in Physics, Chemistry, and Biology*; Maruani, J., Ed.; Kluwer: Dordrecht, The Netherlands, 1989, Vol. 3. Feller, D.; Davidson, E. R. In *Theoretical Models of Chemical Bonding*; Maksic, Z. B., Ed.; Springer: Berlin, 1991; Part 3. Malkin, V. G.; Malkina, O. L.; Salahub, D. R.; Eriksson, L. In *Theoretical and Computational Chemistry*; Politzer, P., Seminario, J. M., Eds.; Elsevier: Amsterdam, 1995; Vol. 2. Chipman, D. M. In *Quantum Mechanical Electronic Structure Calculations with Chemical Accuracy*; Langhoff, S. R., Ed.; Kluwer: Dordrecht, 1995. Ban, F.; Gauld, J. W.; Wetmore, S. D.; Boyd, R. J. In *EPR of Free Radicals in Solids: Trends in Methods and Applications*; Lund, A., Shiotani, M., Eds.; Kluwer: Dordrecht, 2003.

(55) Eriksson, L. A.; Malkin, V. G.; Malkina, O. L.; Salahub, D. R. *Int. J. Quant. Chem.* **1994**, *52*, 879; *J. Chem. Phys.* **1994**, *100*, 5066. Barone, V. *J. Chem. Phys.* **1994**, *101*, 6834. Nguyen, M. T.; Creve, S.; Eriksson, L. A.; Vanquickenborne, L. G. *Mol. Phys.* **1997**, *91*, 537. Feller, D. J. *J. Chem. Phys.* **1990**, *93*, 579. Chen, B.-Z.; Huang, M.-B. *Chem. Phys. Lett.* **1999**, *308*, 256. Engels, B.; Peyerimhoff, S. D. *Mol. Phys.* **1989**, *67*, 583.

(56) Møller, C.; Plesset, M. C. *Phys. Rev.* **1934**, *46*, 618. Frish, M. J.; Head-Gordon, M.; Pople, J. A. *Chem. Phys. Lett.* **1988**, *153*, 503; **1990**, *166*, 275; **1990**, *166*, 281.

(57) Wilson, A.; van Mourik, T.; Dunning, T. H., Jr. *J. Mol. Struct. (THEOCHEM)* **1997**, *388*, 339 and references therein.

(58) Barone, V. In *Recent Advances in DFT Methods, Part I*; Chong, D. P., Ed.; Word Scientific: Singapore, 1996.

(59) Bradforth, S. E.; Jungwirth, P. *J. Phys. Chem. A* **2002**, *106*, 1286.

(60) Bartels, D. M. *J. Chem. Phys.* **2001**, *115*, 4404.

(61) Schlick, S.; Kevan, L. *J. Phys. Chem.* **1977**, *81*, 1083.